

U(As_{1-x}Se_x) solid solutions. I. Resonant x-ray and neutron scattering study of the magnetic phase diagram

M. J. Longfield* and W. G. Stirling*

Department of Physics, Oliver Lodge Laboratory, The University of Liverpool, Liverpool, L69 7ZE, United Kingdom

E. Lidström,[†] D. Mannix,[†] and G. H. Lander

European Commission, JRC, Institute for Transuranium Elements, Postfach 2340, 76125 Karlsruhe, Germany

A. Stunault

European Synchrotron Radiation Facility, Boîte Postale 220X, F-38043 Grenoble, France

G. J. McIntyre

Institut Laue Langevin, Boîte Postale 156, F-38042 Grenoble, France

K. Mattenberger and O. Vogt

Eidgenössische Technische Hochschule, Hönggerberg, Laboratorium für Festkörperphysik, CH-8093 Zürich, Switzerland

(Received 17 July 2000; published 26 February 2001)

We report on a study of the magnetic structure and phase transitions of the UAs_{1-x}Se_x solid solutions employing x-ray and neutron scattering. We have focused this study on compositions $0.18 < x < 0.22$, in which magnetic structures having double-**k** and triple-**k** configurations are found with increasing x . In general, our findings are in excellent agreement with those reported by Kuznietz *et al.* using solely neutron diffraction. However, our x-ray studies have added several important details about (1) the incommensurate transitions near T_N , (2) the nature of the 2**k**-3**k** phase boundary, and (3) the discovery of a new magnetic phase.

DOI: 10.1103/PhysRevB.63.134401

PACS number(s): 75.25.+z

I. INTRODUCTION

The uranium mononictides and monochalcogenides with the fcc rock-salt structure (the “UX” compounds, where X is a pnictide or a chalcogenide) display a fascinating range of magnetic properties and structures.¹ The uranium pnictides ($X = \text{N, P, } \dots, \text{Bi}$) have antiferromagnetic structures in the single-**k**, double-**k**, and triple-**k** (1**k**, 2**k**, 3**k**) classes (see Fig. 1); on traversing the pnictide series with increasing U-U distance, the ordered magnetic moment μ and Néel temperature increase (from $0.75\mu_B$ for UN with $T_N = 50$ K to $2.8\mu_B$ for USb with $T_N = 215$ K). All the uranium chalcogenides are ferromagnets with a $\langle 111 \rangle$ easy axis. Once again, the magnetic properties mirror the increasing U-U distance. US has an ordered moment of $1.7\mu_B$ and a Curie point of 180 K, whereas the corresponding parameters for UTe are $2.25\mu_B$ and 104 K, respectively.¹ The scientific interest in these materials is much enhanced since detailed experiments may be performed on single crystals of the parent compounds as well as solid solutions. For example, antiferromagnetic USb and ferromagnetic UTe form a continuous series of solid solutions, and the magnetism of the USb_{1-x}TeX series has been studied in detail.¹

This paper deals with a systematic study of UAs_{1-x}Se_x single-crystals employing resonant x-ray magnetic scattering (RXMS) and neutron diffraction. The two end member anions, arsenic and selenium, are neighbors in the Periodic Table. The arsenic free atom configuration is $[\text{Ar}] 3d^3 4s^2 4p^3$; selenium has one additional electron in the $4p$ level. The atomic configuration of uranium is $5f^3 6d^1 7s^2$. The

band structure of UAs has been studied by optical spectroscopy.² The $5f$ level lies between the outer $6d$ and inner $4p$ levels, and mixes with the $6d$ and $7s$ levels and the $4p$ level of the anion.

Doping UAs with Se increases the number of electrons in the conduction band and hence alters the environment of the magnetic $5f$ level. Electron hole transitions may take place between the $4p$ and $6d$ level via an exchange with the $5f$ level. UAs and USe both have the NaCl-type crystal structure with similar lattice parameters ($a \sim 5.78$ Å), and hence

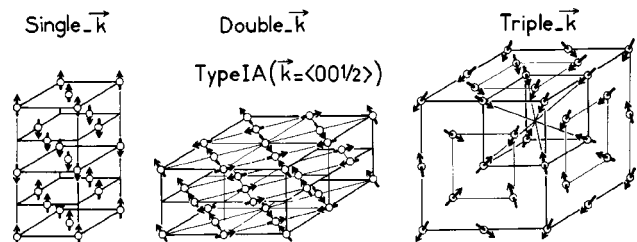


FIG. 1. The multi-**k** structures associated with the actinide rock-salt structure compounds in the type-IA phase. The 1**k** structure is composed of layers of ferromagnetic sheets, which are antiferromagnetically coupled, and for the type-IA (+ + - -) phase the magnetic moments are directed along the propagation vector $\mathbf{k}_3 = [0 \ 0 \ \frac{1}{2}]$. The 2**k** structure is formed by the superposition of two orthogonal propagation vectors, for example, $\mathbf{k}_1 = [\frac{1}{2} \ 0 \ 0]$ and $\mathbf{k}_2 = [0 \ \frac{1}{2} \ 0]$, with the moments in the $(0 \ 0 \ 1)$ plane. The 3**k** structure is made of three orthogonal propagation vectors $\mathbf{k}_1, \mathbf{k}_2, \mathbf{k}_3$ and the moments are oriented along the $\langle 111 \rangle$ directions. (Taken from Ref. 1.)

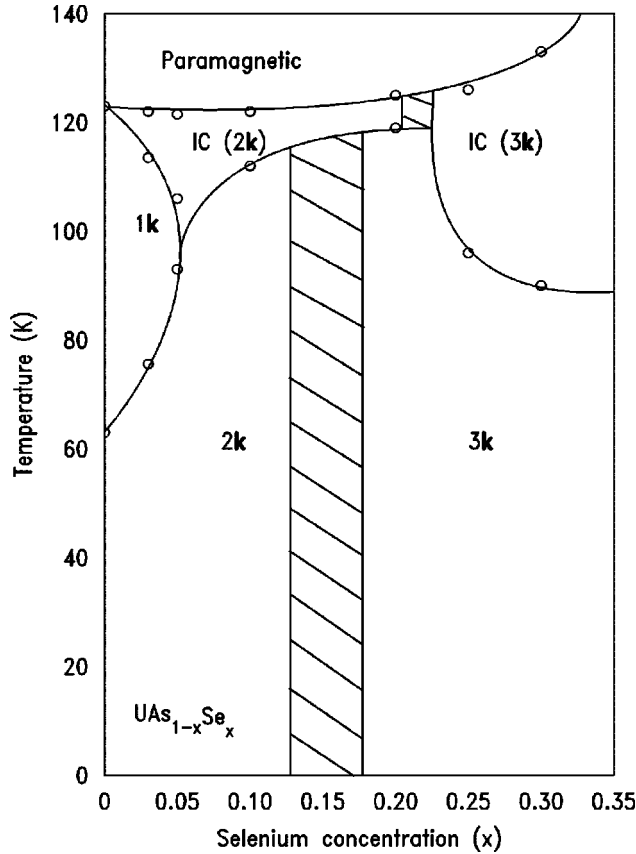


FIG. 2. The magnetic phase diagram (temperature versus composition) of the $\text{UAs}_{1-x}\text{Se}_x$ series of solid solutions as determined by the neutron-diffraction measurements of Kuznietz *et al.* (Ref. 3). The multi- \mathbf{k} structures of the phases were deduced from measurements with finite magnetic fields parallel to the $[1\ 1\ 0]$ direction. IC represents an incommensurate phase. The shaded area is the region of the $2\mathbf{k}$ - $3\mathbf{k}$ phase boundary suggested by Ref. 3.

a continuous series of solid solutions is obtained on mixing the two. The end members of the series display contrasting magnetic properties; UAs is a type-I $1\mathbf{k}$ ($=\langle 0\ 0\ 1 \rangle$) antiferromagnet between 127 K (T_N) and 64 K (T_{IC}). At 64 K there is a second phase transition to a type-IA $2\mathbf{k}$ structure ($\mu = 2.2\mu_B$). The net magnetic moments are aligned along $\langle 1\ 1\ 0 \rangle$ directions and the magnetic modulation wave vector is $\langle 0\ 0\ \frac{1}{2} \rangle$. USe transforms at $T_C = 160$ K to a $\langle 1\ 1\ 1 \rangle$ easy-axis ferromagnet with $\mu = 2.0\mu_B$. Neutron-diffraction measurements of $\text{UAs}_{1-x}\text{Se}_x$, by Kuznietz *et al.*,³ have shown a rich series of magnetic structures for $x < 0.35$ with incommensurate phases near T_N , and commensurate phases with $2\mathbf{k}$ and $3\mathbf{k}$ structures at lower temperature (see Fig. 2). The incommensurate modulation wave vector $[0\ 0\ k]$ varies with concentration and temperature. Commensurate phases exist at low temperature with multi- \mathbf{k} configurations which depend upon the selenium concentration. At low temperature the $2\mathbf{k}$ type-IA ($++--$) structure occurs and is the only commensurate phase for $x < 0.15$. At higher temperatures an incommensurate phase exists. For $0.20 < x < 0.35$ the low-temperature stable phase was proposed to have a $3\mathbf{k}$ configuration, again with the wave vector $\mathbf{k} = \langle 0\ 0\ \frac{1}{2} \rangle$. For

$0.35 < x < 0.45$ complex antiferromagnetic structures exist and for $x > 0.45$ ferromagnetism is found. Our study is confined to the region $0.10 < x < 0.25$ in which some of the interesting phase transitions, particularly those between different multi- \mathbf{k} configurations, take place.

II. EXPERIMENT

The crystals were grown at the Laboratorium für Festkörperphysik, Eidgenössische Technische Hochschule Zurich. The average size of the samples was $\sim 3 \times 3 \times 2$ mm³. The full width at half maximum (FWHM) of the rocking curve of the charge $(0\ 0\ 2)$ reflection measured at 3.73 keV was about 0.05° . The first set that we examined ($0 < x < 1$) came from the same batch of crystals for which the neutron studies were made.³ A newer batch of crystals of similar composition ($x = 0.18$ and 0.20) was also studied. The RXMS experiments were carried out at the ID20 beam line of the European Synchrotron Radiation Facility (ESRF), Grenoble, France, and the X22C beam line at the National Synchrotron Light Source, BNL, USA. For magnetic measurements the x-ray energy was tuned to the uranium M_4 absorption edge (3.73 keV). Detailed measurements of the crystal lattice were carried out using the XMaS beam line at the ESRF with a photon energy of 8 keV and a Ge(1 1 1) analyzer in the scattered beam to improve the resolution. Neutron-diffraction measurements were performed with the D10 four-circle diffractometer at the Institut Laue Langevin, Grenoble, France. Neutrons with a wavelength of 2.36 Å were selected using a pyrolytic graphite $(0\ 0\ 2)$ monochromator. The $\lambda/2$ contamination was suppressed with a graphite filter.

III. MAGNETIC PHASES NEAR T_N

The solid solutions for $x < 0.10$ have been studied by Kuznietz *et al.*³ and we have not reexamined these samples. Our primary interest is in the region where the $2\mathbf{k}$ changes into the $3\mathbf{k}$ structure as a function of x . We show in Fig. 3 reciprocal space scans along \mathbf{c}^* around $(0\ 0\ 2+k)$ as a function of temperature for the $x = 0.10$ sample. In agreement with Ref. 3, T_N is of order 122 K, and we confirm that there is a coexistence of the incommensurate ($k > 0.5$) and type-IA ($k = 1/2$) phases, suggesting a discontinuous phase transition between these two, as also suggested in Ref. 3. In this sample the value of δ_{inc} (defined as the incommensurate wave vector offset at T_N ; $k_{inc} = 1/2 + \delta_{inc}$) has a value of 0.047. The excellent wave vector resolution of the x-ray technique is especially useful when there are coexisting modulations, as in the case of Fig. 3. For the $x = 0.15$ sample, a rather similar situation occurs except that the value of δ_{inc} in this sample is 0.025 at T_N . For the $x = 0.18$ sample, scans along \mathbf{c}^* are shown in Fig. 4. Here T_N is somewhat reduced (to ~ 120 K), but the more interesting aspect is that there is no sign of an incommensurate phase, i.e., $\delta_{inc} = 0$. This feature is not apparent from the Kuznietz *et al.*³ phase diagram (see Fig. 2) but is implicit in their Fig. 10, which shows k as a function of x . The situation for concentrations close to, but above $x = 0.18$, is shown in Fig. 5 for $x = 0.20$. Here we note that $\delta_{inc} = -0.025$ at $T_N = 125$ K. These results agree well

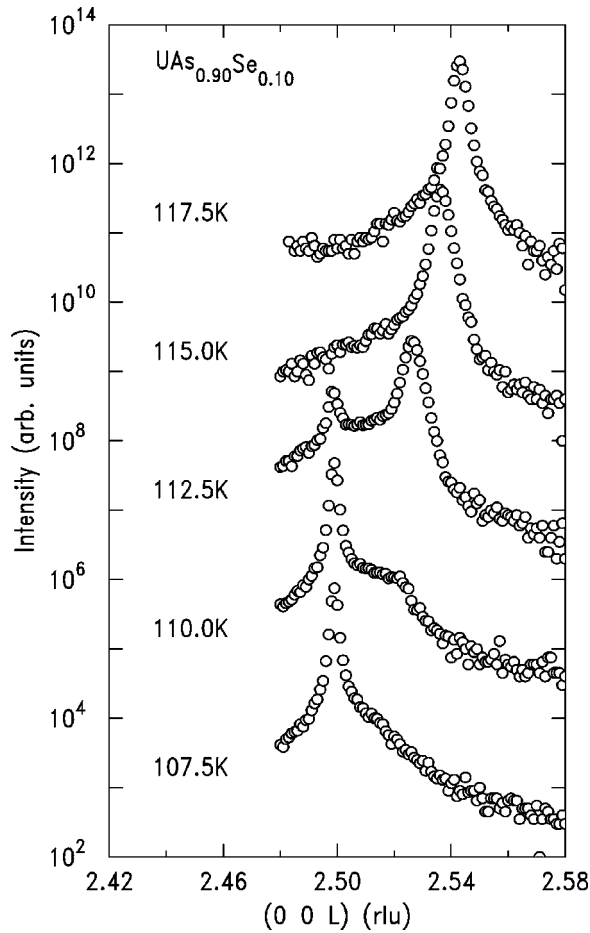


FIG. 3. RXMS reciprocal space scans along \mathbf{c}^* for $\text{UAs}_{0.90}\text{Se}_{0.10}$ at decreasing temperatures through the incommensurate-commensurate phase transition. Data at successive temperatures have been shifted by an order of magnitude for presentation (X22C). Note the logarithmic intensity scale.

with those obtained by neutron diffraction, but we establish more clearly the lack of an incommensurate phase in the $x=0.18$ sample.

IV. COMMENSURATE PHASES

A. Domain effects

In standard diffraction experiments, an assembly of $1\mathbf{k}$ magnetic domains cannot be distinguished from a multi- \mathbf{k} structure.¹ It is possible, however, to make the distinction by applying a symmetry breaking magnetic/electrical/stress field, which would favor a particular domain. Rossat-Mignod *et al.*⁴ showed that uniaxial stress may lead to the change of the domain population from their study of UN, UAs, and USb. For example, if $c/a < 1$ and a uniaxial stress is applied in the $[0\ 0\ 1]$ direction, then the domains with $\mathbf{k}=[0\ 0\ 1]$ will be favored as the stress will reduce the length in the c direction at the expense of the other two directions. It is also possible to detect a change in the domain population when the x-ray probe does not average over a large number of domains. This is the situation for RXMS,⁵ where the penetration depth for uranium compounds (employing an x-ray en-

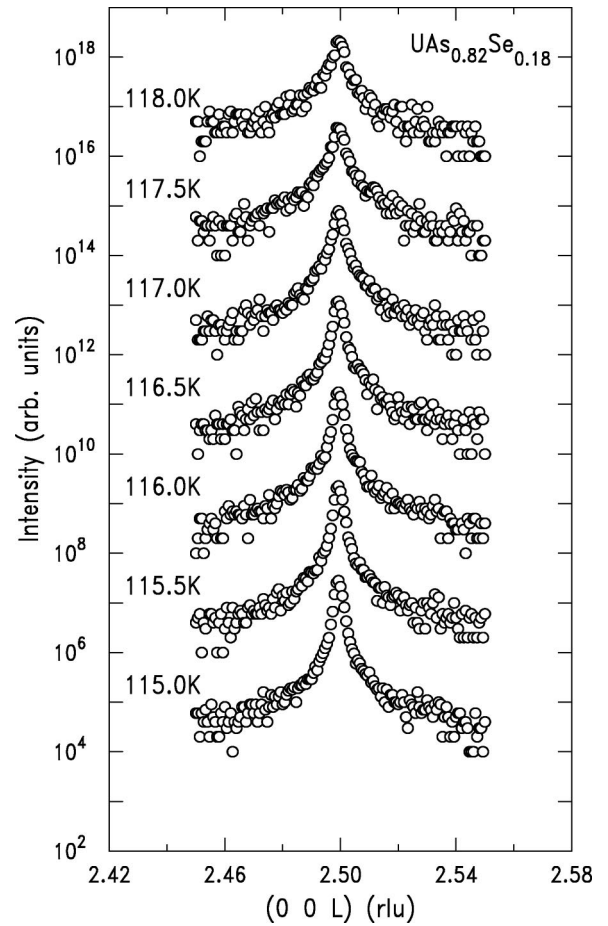


FIG. 4. RXMS reciprocal space scans along \mathbf{c}^* for $\text{UAs}_{0.82}\text{Se}_{0.18}$ at decreasing temperatures. No incommensurate phase was observed. Data at successive temperatures have been shifted by an order of magnitude for presentation (X22C).

ergy of 3.73 keV, the $\text{U } M_4$ edge) is of the order of 1000 Å, in contrast to neutron scattering, which is a bulk probe and thus averages over many domains. Of course, the x-ray method depends on the domain size, so if no effect is seen it does not necessarily imply that the structure is $3\mathbf{k}$. Such an effect is shown in Fig. 6 for the $x=0.20$ crystal. From T_N to 60 K the variation of the intensities from potentially different domains are the same, whereas they are very different below 60 K.

The intensity differences below 60 K may be understood qualitatively by assuming a transition from a $3\mathbf{k}$ ($T > 60$ K) to a $2\mathbf{k}$ state ($T < 60$ K). In the $2\mathbf{k}$ structure (see Fig. 1), there are domains corresponding to the magnetic moment components along different directions. In the $2\mathbf{k}$ structure, the domains contributing to the intensity at $(0\ 0\ 2.5)$ have resultant components along $[0\ 1\ 1]$ and $[1\ 0\ 1]$, and we specify the population of these domains as $p(yz)$ and $p(xz)$. In all there are 12 domains corresponding to moments along all equivalent $\langle 1\ 1\ 0 \rangle$ directions, but we may restrict these to three domains with populations $p(xy)$, $p(yz)$, and $p(zx)$ without loss of generality. If each of these populations is $1/3$, then the measured intensities will be equal, apart from geometrical factors. If $p(xy)$ increases from 0.33 to 0.6 and

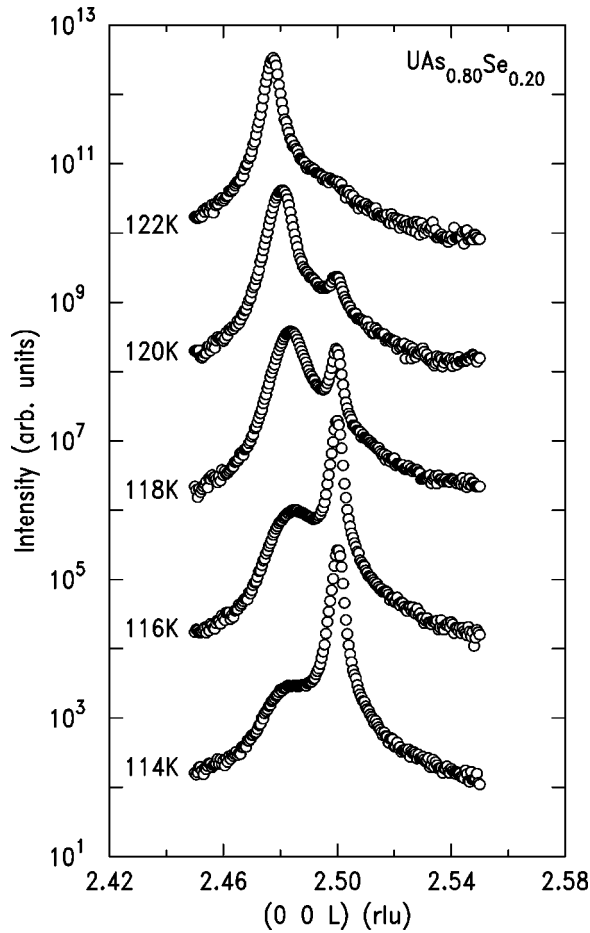


FIG. 5. RXMS reciprocal space scans along c^* for $\text{UAs}_{0.80}\text{Se}_{0.20}$ at decreasing temperatures through the incommensurate-commensurate phase transition. Data at successive temperatures have been shifted by an order of magnitude for presentation (ID20). For clarity only some of the scans are shown.

$p(yz) = p(zx)$ both decrease from 0.33 to 0.2, then the corresponding reflections $(0\ 0\ 2+k)$ and $(k\ 0\ 2)$ would have relative intensities of approximately 0.4 and 0.8, respectively, which gives the factor of 2 difference in intensity, shown in Fig. 6. This suggests that for $x=0.20$ the magnetic structure is not $3\mathbf{k}$ below 60 K, but possibly $2\mathbf{k}$.

B. External tetragonal distortions and volume effects

Actinide compounds with the rock-salt structure typically display magnetostriction effects that are the result of the coupling of the orbital moments with the crystal lattice. McWhan *et al.* studied a UAs single crystal and observed several magnetostrictive effects.⁵ A change of $\delta a/a = 1.5 \times 10^{-4}$ was observed in the lattice parameter as the magnetic structure changes from type-I $1\mathbf{k}$ to type-IA $2\mathbf{k}$. This is in agreement with a previous measurement⁶ of the volume expansion that gave a value of $(1/3) \delta V/V = 1.3 \times 10^{-4}$. A tetragonal distortion of $c/a = 1.0002$ about the $(0\ 0\ 6)$ position corresponding to $(c-a)/c = 2.0 \times 10^{-4}$ was also found. Finally, a $2\mathbf{k}$ charge modulation was observed from the type-IA structure that corresponds to an internal displacement of the atomic positions of $\delta x = 0.002\ \text{\AA}$.

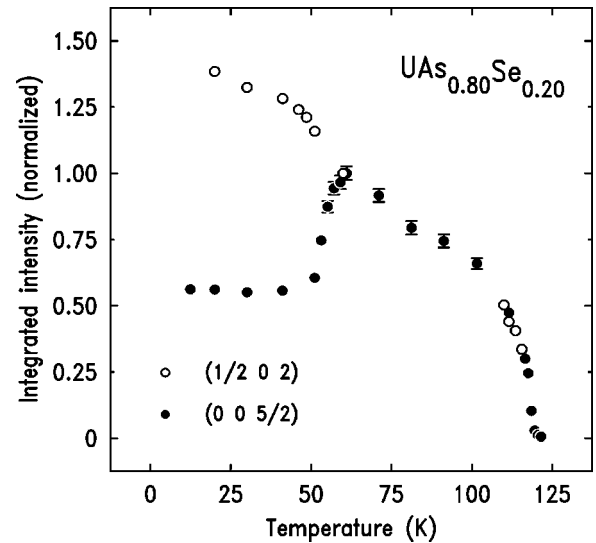


FIG. 6. The temperature dependence of the integrated intensity for the specular $(0\ 0\ 2+k)$ and off-specular $(k\ 0\ 2)$ commensurate ($k=1/2$) magnetic satellites of $\text{UAs}_{0.80}\text{Se}_{0.20}$ represented by closed and open symbols, respectively. The data have been normalized at 60 K (ID20).

We have studied the temperature dependence of the $(0\ 0\ 6)$ charge reflection for the $x=0.18, 0.20, 0.22,$ and 0.25 compositions of the $\text{UAs}_{1-x}\text{Se}_x$ series. An example of the reciprocal space scans is given for the $x=0.18$ crystal in Fig. 7(a). In the paramagnetic phase, the crystal has cubic symmetry and there is a single charge peak. The same is true between T_N ($\sim 125\ \text{K}$) and $T^* \sim 60\ \text{K}$. The latter is defined as the lowest temperature for which the lattice appears cubic. Below T^* the single lattice Bragg reflection develops into two peaks split along the L direction about the $(0\ 0\ 6)$ position [see Fig. 7(b)]. This double peaked reflection results from the two different lattice parameters a (and b) and c . In the analysis, the two lattice peaks about the $(0\ 0\ 6)$ position have each been modeled by Lorentzian functions. The fit to the low temperature reflections gives a distortion of $0.0014\ \text{rlu}$ at the $(0\ 0\ 6)$ position for $\text{UAs}_{0.82}\text{Se}_{0.18}$, which gives a value for $(c-a)/c$ of $\sim 2.3 \times 10^{-4}$. The temperature dependencies of the lattice distortion for three values of the selenium composition x are shown in Fig. 8. The $x=0.25$ crystal does not distort at low temperature. Details of the tetragonal distortions are given in Table I.

In lowering the symmetry from cubic to tetragonal (as shown in Fig. 8) there is a change in the cell volume, which may be characterized as $\delta a/a$. The value $\delta a/a$ was determined from the difference between the lattice parameter in the cubic phase and the average lattice parameter in the tetragonal phase; the results are shown in Table I.

C. Internal distortions

As can be seen from Fig. 1, the magnetic structures of these materials consist of Fourier components propagating along the cubic $\langle 0\ 0\ 1 \rangle$ directions with the moment directions perpendicular to the propagation direction. This gives rise to planes in which the Fourier components of the moment are

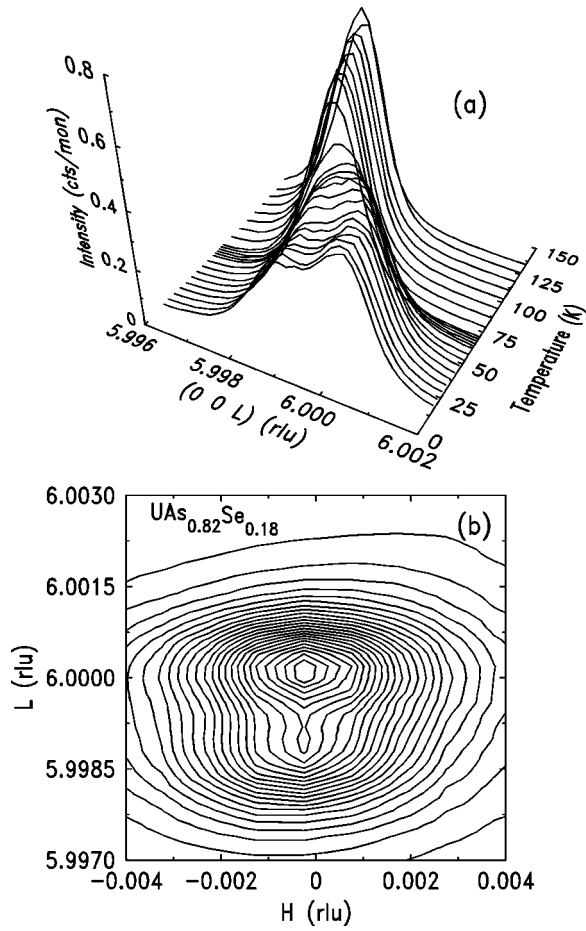


FIG. 7. (a) Reciprocal space scans for UAs_{0.82}Se_{0.18} about the (0 0 6) lattice reflection at decreasing temperatures. (b) Contour plot around the (0 0 6) lattice position at 12 K (XMaS).

perpendicular to the plane. An interesting magnetostrictive effect is due to a small difference in the separation between the ++ moment planes and those oppositely directed +-. Unlike the external tetragonal distortion discussed above, this effect is independent of the multi- \mathbf{k} nature of the magnetic structure, and may exist in all configurations below T_N . The difference in separation between the planes induces a distortion internal to the unit cell with a periodicity of twice the magnetic wave vector. If $k = 1/2$, this produces a charge

TABLE I. T^* is the temperature range over which the lattice peak begins to broaden and the lattice distortion at low temperature (12 K) is given as $(c-a)/c$. The volume change $\delta a/a$ upon lowering the temperature from the cubic to the tetragonal phase is given. The errors in $(c-a)/c$ and $\delta a/a$ are to within 20%.

x	T^* (K)	$(c-a)/c$ (10^{-4})	$\delta a/a$ (10^{-4})
0.00 ^a	~62	2.0	1.5
0.18	~60	2.3	3.9
0.20	49–54	1.9	16.7
0.22	55–63	1.7	0.07

^aReference 5.

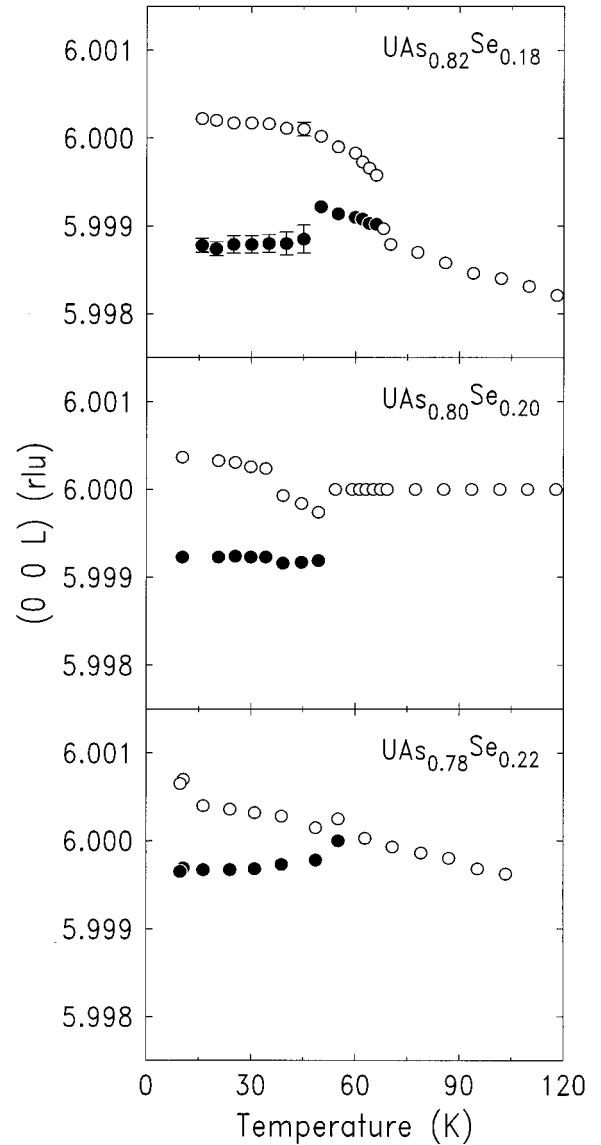


FIG. 8. Results from the analysis of reciprocal space scans about the (0 0 6) lattice point at decreasing temperatures for UAs_{1-x}Se_x with $x=0.18, 0.20,$ and 0.22 . At temperatures down to about 60 K the crystal lattice has cubic symmetry, whereas below this temperature the lattice is tetragonal. The open and closed symbols correspond to the a (and b) and c lattice parameters, respectively (XMaS).

reflection at forbidden lattice positions, e.g., (0 0 3). An example, for the $x=0.18$ sample, is shown in Fig. 9. Similar peaks were observed in all samples in the ordered phase. Unlike the lattice reflection, a double peak is *not* observed at the (0 0 3) position because the magnetic propagation of the $2\mathbf{k}$ structure is *only* along the a and b directions. The position of the lattice modulation corresponds to the position of the larger scattering vector of the lattice reflection for all of the UAs_{1-x}Se_x crystals studied, which gives $c/a > 1$ in the tetragonal phase. This is in agreement with uniaxial stress measurements⁴ and the x-ray scattering measurements of McWhan *et al.*⁵ on UAs.

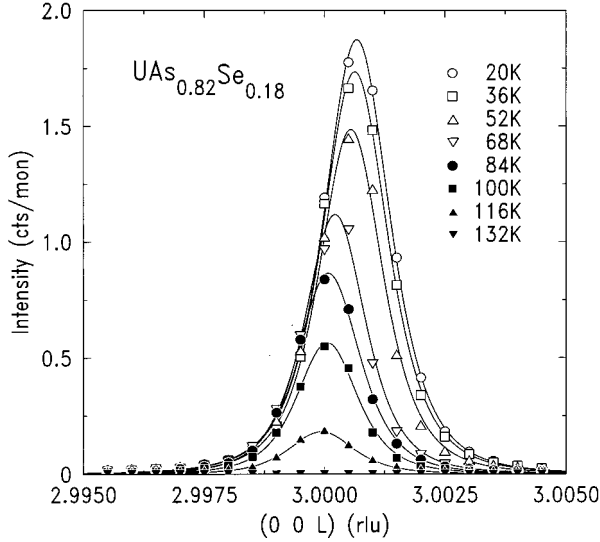


FIG. 9. Reciprocal space scans along c^* at decreasing temperatures at the “forbidden” Bragg position $(0\ 0\ 3)$ for $\text{UAs}_{0.82}\text{Se}_{0.18}$. The charge diffraction peak at $(0\ 0\ 3)$ results from atomic displacements internal to the unit cell (XMaS).

The amplitude of charge scattering from the lattice modulation is proportional to the internal displacement of the uranium atoms *within* the unit cell. For UAs the displacement⁵ is $\delta x = 0.002\ \text{\AA}$. We have attempted to calibrate the internal distortion amplitude δx in our samples by comparing the intensity of the $(0\ 0\ 3)$ to the very strong charge $(0\ 0\ 4)$. Within the considerable errors bars associated with this normalization, we find a value similar to the $\delta x = 0.002\ \text{\AA}$ reported for UAs.

V. NEW MAGNETIC PHASE

Using RXMS at the uranium M_4 edge, we have discovered a feature of the $\text{UAs}_{1-x}/\text{USe}_x$ phase diagram. An extra diffraction peak coexists with the main commensurate satellites at low temperatures ($T < 60\ \text{K}$). This feature, which has been observed in x-ray measurements for each of the $x = 0.18, 0.20,$ and 0.22 crystals, is shown in Fig. 10(a) for the $x = 0.20$ sample. As the temperature is lowered the position of the incommensurate peak moves away from the commensurate position and increases in intensity to become approximately 1% of the main commensurate peak at low temperature. To confirm these results, a second $x = 0.20$ sample was grown, and identical results were obtained.

The incommensurate peak was also observed at off-specular positions, i.e., $(k\ 0\ 2)$. The wave vectors of the new satellites in the $x = 0.18$ and 0.22 samples are similar to those found in the $x = 0.20$ sample, but do not exist down to low temperature. Table II gives the temperatures and compositions that form the boundary of this new phase.

At first sight, it is not clear if this extra diffraction peak originates from the charge or magnetization, surface or bulk of the sample. To determine whether the extra peak really comes from the bulk of the sample, we have performed neutron experiments on the D10 diffractometer at the Institut

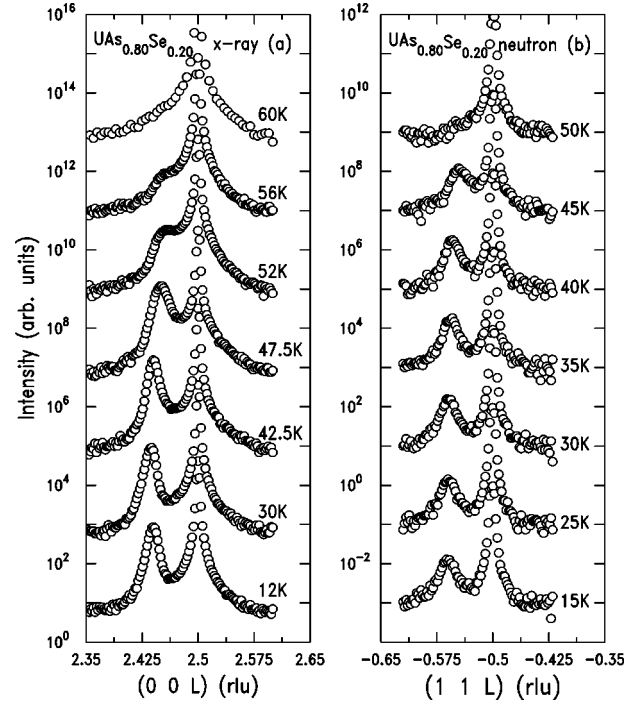


FIG. 10. (a) RXMS reciprocal space scans for $\text{UAs}_{0.80}\text{Se}_{0.20}$ at decreasing temperatures in the commensurate phase. (b) Neutron scattering reciprocal space scans for $\text{UAs}_{0.80}\text{Se}_{0.20}$ at decreasing temperatures in the commensurate phase. Both techniques demonstrate that an extra diffraction peak develops at $k_m \sim 0.44$ which varies in intensity, width, and position on lowering the temperature.

Laue Langevin on the *same* $x = 0.2$ sample as used in the x-ray experiments. The results are shown in Fig. 10(b). They confirm that both reflections originate from the bulk of the sample, and the maximum intensity of the extra modulation is $\sim 1\%$ of the main $k = 1/2$ peak in both x-ray and neutron studies. An additional method of determining the spatial location of the magnetic modulation giving rise to a new diffraction peak is to examine its dependence on incident photon energy with the RXMS technique.⁷ The resonant enhancements (at the $\text{U}\ M_4$ absorption edge) of the commensurate peak ($k = 0.5$) and of the “extra” peak ($k_m \sim 0.44$) are compared in Fig. 11. The scattering intensity for the two peaks has been normalized and shows clearly that the magnetic signal from both peaks is enhanced, and at the same energy. The extra peak is therefore considered as a magnetic modulation of the main commensurate $++--$ structure.

TABLE II. The range of temperatures and wave vectors that characterize the low temperature incommensurate magnetic modulation.

x	T_M (K)	k (rlu)
0.18	35–55	0.44–0.47
0.2	12–58	0.44–0.47
0.2 (new)	12–58	0.44–0.47
0.22	40–55	~ 0.45

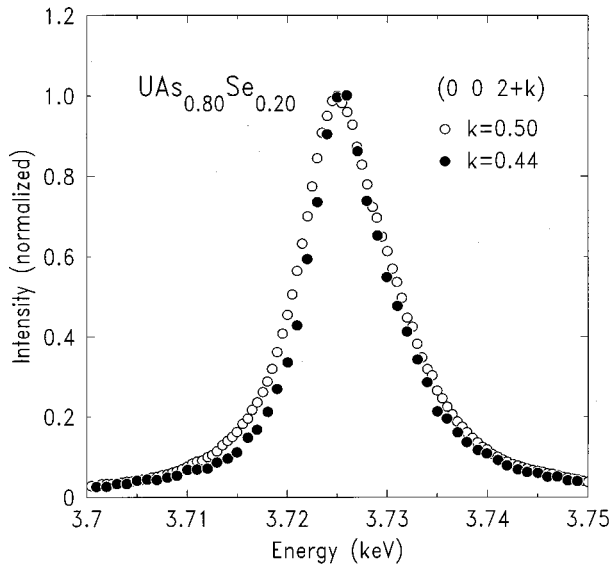


FIG. 11. X-ray energy dependence of the commensurate ($k = 1/2$; open symbols) and incommensurate ($k_m = 0.44$; closed symbols) diffraction peaks for $\text{UAs}_{0.80}\text{Se}_{0.20}$ at 12 K. These data have been normalized at the peak position (ID20).

The slightly different energy widths may be related to the absence of a completely long-range ordered peak at $k \sim 0.44$, since its width in momentum space is considerably greater than that of the main modulation.

VI. SUMMARY

We have reported in this paper a series of RXMS measurements on $x = 0.10, 0.18, 0.20, 0.22,$ and 0.25 samples of the $\text{UAs}_{1-x}\text{Se}_x$ solid solutions. In general, our findings are in excellent agreement with those reported by Kuznietz *et al.* using neutron diffraction.³ This is expected as many of our samples are the same ones as used in the neutron study. However, the x-ray studies have added the following important details.

A. Incommensurate transitions near T_N

As summarized in Fig. 6 there is a distinct change at $x = 0.18$ when the extent of the incommensurability changes from $\delta_{inc} > 0$ (for $x < 0.18$) to $\delta_{inc} < 0$ (for $x > 0.18$), where the wave vector $k = 1/2 + \delta_{inc}$. All systems for $x < 0.25$ adopt the $k = 1/2$ magnetic structure at low temperature. For $x = 0.18$ there is no incommensurate phase (see Fig. 4).

B. Nature of the 2k and 3k phase boundaries

The boundary between the 2k and the 3k magnetic phases can be determined by applying a magnetic field in a neutron diffraction experiment. This is more difficult in x-ray experiments where complementary methods involve comparing different reflections and searching for lattice distortions as a function of temperature. Since the probing depth of RXMS is only about 1000 Å it is possible for the 1k and 2k structures [both of which involve domains (see Fig. 1)] that

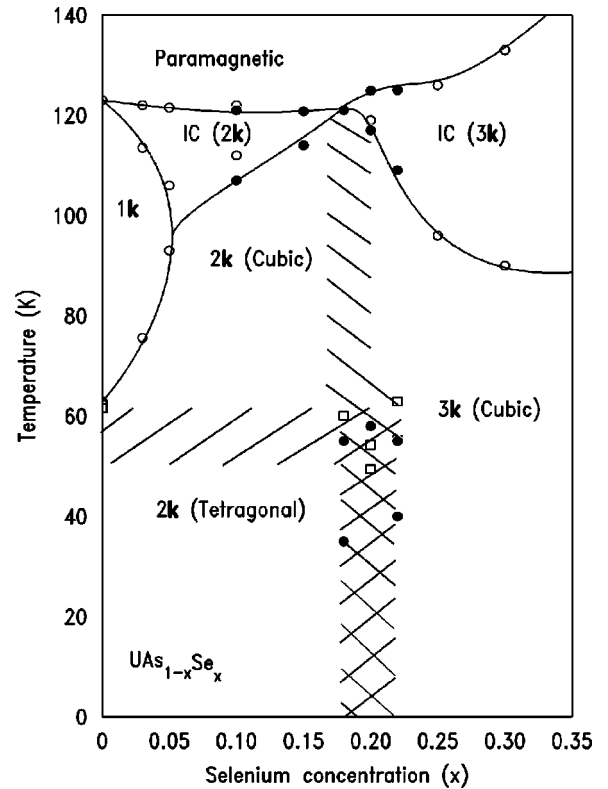


FIG. 12. The modified magnetic phase diagram (temperature versus composition) of the $\text{UAs}_{1-x}\text{Se}_x$ series of solid solutions in zero applied magnetic field determined by the present RXMS (closed circles) and neutron diffraction measurements (open circles) of Kuznietz *et al.* (Ref. 3). The multi- \mathbf{k} structures of the different phases were deduced from neutron measurements with finite magnetic fields (Ref. 3), and from x-ray charge scattering (open squares) to deduce the lattice symmetry, as discussed in the text. The phase discovered in this work is shown as a cross-hatched region.

different temperature dependencies may be observed for nominally equivalent reflections. Such differences may arise from probing different domains, even though they average over the total volume. A good example of these effects was shown in the study⁸ of NpAs and is shown for the $x = 0.20$ sample in our study in Fig. 6. The similar temperature dependencies for $T > 60$ K suggests (but does not prove) that the structure is 3k. The inequivalence for $T < 60$ K proves that the structures cannot be 3k in this temperature range. A less ambiguous way to establish the multi- \mathbf{k} nature is to examine the lattice symmetry. This is demonstrated in Figs. 8 and 9. The samples with $x = 0.18, 0.20,$ and 0.22 all show a tetragonal distortion at $T^* \sim 60$ K. Below this temperature they cannot be 3k (which has cubic symmetry), and since this temperature (T^*) is close to that at which pure UAs transforms into the type-IA ($k = 1/2$) phase, we propose a line across the new phase diagram (Fig. 12) separating the low temperature 2k phase from the phases at higher temperature. The magnitudes of the tetragonal distortions appear independent of x , as shown in Table I.

Another magnetostrictive effect is related to an internal distortion of the planes so that the distance between the

planes with parallel magnetic moments is different to that where the moments are antiparallel. This effect was predicted by Cooper⁹ and first observed by McWhan *et al.*⁵ in UAs. We observe this internal distortion for all our samples; the effect does not depend on the multi- \mathbf{k} nature of the magnetic structure. As shown in Fig. 9, the internal distortion appears just below T_N and has its greatest magnitude at low temperature, as expected. This modulation, which may be thought of as a charge-density wave, has a periodicity twice that of the magnetic modulation.

C. Observation of a new phase

Our experiments have led to the observation of an “extra” magnetic peak within what would appear to be a stable type-IA structure. This is shown for $x=0.20$ in Fig. 10. It is seen in the $x=0.18$, 0.20, and 0.22 samples with its maximum intensity close to 50 K, and with similar modulation

wave vectors. We have verified that (1) it is *magnetic* by measuring the intensity dependence as a function of incident photon energy, (2) that it is found in a *freshly made* $x=0.20$ sample, and (3) that it exists in the *bulk* of the sample, as it can be observed with high-resolution neutron diffraction [Fig. 10(b)]. The part of the phase diagram where this new “phase” has been observed is shown hatched in Fig. 12. A possible origin for this unusual peak is discussed in Ref. 10.

ACKNOWLEDGMENTS

M.J.L. and W.G.S. are grateful to the UK Engineering and Physical Science Research Council for financial assistance. E.L. and D.M. thank the European Commission for funding under the Training and Mobility of Researchers program. Work at Brookhaven was supported by the U.S. DOE under Contract No. DE-AC02-98CH10886.

*Present address: European Synchrotron Radiation Facility, B.P. 220X, F-38043 Grenoble, France.

†Also at ESRF, B.P. 220X, F-38043 Grenoble, France.

¹J. Rossat-Mignod, G.H. Lander, and P. Burlet, *Handbook on the Physics and Chemistry of the Actinides* (North-Holland, Amsterdam, 1984), Vol. 1, Chap. 6, p. 415.

²W. Reim, J. Schoenes, and O. Vogt, *Phys. Rev. B* **29**, 3252 (1984).

³M. Kuznietz, P. Burlet, J. Rossat-Mignod, and O. Vogt, *J. Magn. Mater.* **69**, 12 (1987).

⁴J. Rossat-Mignod, P. Burlet, H. Bartholin, R. Tchapoutian, O. Vogt, C. Vettier, and R. Lagnier, *Physica B* **102**, 177 (1980).

⁵D.B. McWhan, C. Vettier, E.D. Isaacs, G.E. Ice, D.P. Siddons,

J.B. Hastings, C. Peters, and O. Vogt, *Phys. Rev. B* **42**, 6007 (1990).

⁶H.W. Knott, G.H. Lander, M.H. Mueller, and O. Vogt, *Phys. Rev. B* **21**, 4159 (1980).

⁷N. Bernhoeft, A. Hiess, S. Langridge, A. Stunault, D. Wermeille, C. Vettier, G.H. Lander, M. Huth, M. Jordan, and H. Adrian, *Phys. Rev. Lett.* **81**, 3419 (1998).

⁸S. Langridge, W.G. Stirling, G.H. Lander, and J. Rebizant, *Phys. Rev. B* **49**, 12 022 (1994).

⁹B.R. Cooper, *Phys. Rev. B* **17**, 293 (1978).

¹⁰M.J. Longfield, W.G. Stirling, and G.H. Lander, *Phys. Rev. B* **63**, 134402 (2001).